Tunneling nanotubes propagate a BMP-dependent preneoplastic state.

Cristina Cuella Martin[1,2,3], Thanh Thuy Nguyen *[1,2,3], Alexia Bertin *[1,2,3], Kevin Geistlich[1,2,3,4], Boris Guyot[1,2,3], Sylvain Lefort[1,2,3], Emmanuel Delay[1,2,3,4], Charline Dalverny[3,5], Alice Boissard[6], Cécile Henry[6], François Guillonneau[6,7,8], Eve-Isabelle Pécheur §*[1,2,3] and Véronique Maguer-Satta §*[1,2,3,4]

1. CNRS UMR5286, Centre de Recherche en Cancérologie de Lyon, 69008 Lyon, France;
2. Inserm U1052, Centre de Recherche en Cancérologie de Lyon, 69008 Lyon, France;
3. Université Claude Bernard Lyon 1, Lyon, France;
4. Centre Léon Bérard, 69008 Lyon, France;
5. Centre Technologique des Microstructures (CTμ), 69622 Villeurbanne, France;
6. Prot'ICO proteomics facility, Institut de Cancérologie de l'Ouest, 49055 Angers, France,
7. Nantes Université, Inserm, CNRS, CRCI2NA, U1307, UMR6075, 44000 Nantes, France;
8. Equipe Labellisée Ligue Contre le Cancer, Paris, France.

* These authors contributed equally; § Co-corresponding authors

Co-corresponding authors: Eve-Isabelle PÉCHEUR and Véronique MAGUER-SATTA, Centre de Recherche en Cancérologie de Lyon-CRCL, UMR CNRS 5286/Inserm U1052, 28 rue Laënnec, 69373 Lyon Cedex 08, France; 33-4-7878-2907 or 33-4-7878-2806.
Emails: eve-isabelle.pecheur@inserm.fr ; veronique.maguer-satta@lyon.unicancer.fr

Keywords: Tunneling nanotubes, cell communication, preneoplasia, BMP, breast cancer initiation.

Abstract.

Tunneling nanotubes (TNTs) are thin, actin-rich structures that facilitate long-distance intercellular communication through the transfer of molecules and organelles. While their role in cancer progression is well-established, their involvement in the earliest stages of tumor initiation remains unexplored. Using normal human mammary primary cells, a model of early luminal breast transformation, and mammary organoids, we demonstrate that TNTs become increasingly abundant and elongated during the initial phases of luminal breast cell transformation. Notably, these structures preferentially connect transformed donor cells to non-transformed acceptor cells, establishing a directional communication network. Unbiaised proteomic analyses and (correlative) super-resolution microscopy reveal that, through this network, transformed cells transfer key molecular signals to non-transformed acceptor cells, inducing changes of their proteome landscape within days. Further analyses of acceptor cells reveal dysregulation of the BMP pathway, including increased expression of the Bone Morphogenetic Protein receptor type 1b (BMPR1b), together with functional phenotypic alterations such as the acquisition of anchorage-independent growth, a hallmark of preneoplastic progression. Our findings highlight how TNT-mediated transfer initiates a BMP-dependent cascade of molecular and phenotypic changes in acceptor cells, effectively propagating a preneoplastic state within the luminal breast epithelium. By elucidating these early events, we provide novel insights into the mechanisms underlying the onset and spread of epithelial transformation in luminal breast cancer, underpinning the key role of the BMP pathway, and offering new avenues for understanding how preneoplastic states emerge and disseminate.

With 2.3 million women affected worldwide and 700,000 deaths per year, breast cancer is the leading cause of cancer-related death in women, with luminal types representing 70% of all cases [1], and ductal carcinoma *in situ* (DCIS) the earliest non-invasive stage. The Bone Morphogenetic Proteins (BMP) pathway is a key actor altered during luminal breast tumorigenesis [2–4]. Together with an interleukin-6 (IL6)-mediated inflammation, enhanced BMP2 secretion by the niche surrounding mammary stem cells fuels their transformation into cancer stem cells *via* amplification of their response to the kinase BMP receptor type 1b (BMPR1b), without detectable genetic alterations [3,5]. Cancer stem cells can drive tumorigenesis and chemoresistance through exogenous signaling pathways that maintain their stemness and promote survival [6,7]. BMPR1b-silenced transformed mammary cells have drastically decreased capacities to initiate tumor formation *in vivo* [3]. However, the early dynamics of BMP-mediated transformation and the evolution of non-transformed mammary cells towards tumor cells remain unexplored.

Tunneling nanotubes (TNTs) are thin, transient actin-based structures enabling long-range intercellular communication [8,9], *via* the transfer of organelles, small molecules, proteins and nucleic acids. TNTs have been implicated in tumor progression, metastasis, and chemoresistance. Cancer cells linked to neurons by TNTs exhibited enhanced metastatic capacities [10–12]. Yet the role of TNTs at earliest stages of tumorigenesis is unknown.

While BMPs and TNTs have independently been associated with breast cancer, their potential interaction is unexplored. Also, the nature, directionality, and functional consequences of cell/cell communications at the tumor initiation stage remain ill-defined.

In this work, we aimed to delineate the interplay between the BMP pathway and TNT-mediated communication, to shed light on the earliest steps of transformation of (immature) mammary cells.

75 **Results.**

76 **TNT formation during mammary epithelial stem cells transformation.**

77 Early BMP-driven transformation dynamics was explored by using our clinically-relevant
78 MCF10A-derived stem cell models, obtained by chronic exposure to IL6 and BMP2 (MC26
79 and M1B26; Figure 1A) [3,5]. Sorting of BMPR1b-expressing cells prior to cytokine treatment,
80 followed by soft agar clones selection, led to quicker establishment of transformed cells
81 (M1B26), with greater *in vitro* anchorage-independent growth and *in vivo* engraftment than in
82 non BMPR1b-sorted cells (MC26). These models display DCIS molecular features and robustly
83 recapitulate the *in vivo* BMP pathway alterations [3,5]. Super-resolution Airyscan confocal
84 microscopy observations of non-transformed control (MCF10A-CT) and transformed cells
85 (MC26, M1B26) revealed long-range contacts *via* long thin F-actin-rich TNTs [13] (Figure 1B).
86 Although TNT quantification requires low-confluence cultures [14], long-range TNTs were also
87 detectable at high cell density (Figure S1A). Transformed cells exhibited over twice as many
88 TNTs as non-transformed cells (Figure 1C, left). The proportion of long TNTs increased
89 ~fivefold with transformation (Figure 1C, right). However, TNT average length did not differ
90 between cell lines (Figure S1B). Neither TNT number nor length varied in non-transformed
91 cells exposed to conditioned medium of transformed ones (Figure S1B-D). As observed by
92 scanning electron microscopy, TNTs in transformed cells were often branched, with
93 ramifications and bulges (Figure 1D black arrow) [8,13]. While most TNTs were open-ended,
94 allowing a cell-cell cytoplasmic continuum (Fig. 1E), some close-ended TNTs featuring a Gap
95 junction at one tip were seen (Figure S1E). TNTs did not adhere to the substrate and were
96 observed within 3D structures such as acini (Figure 1F), basic functional units of breast
97 glandular tissue (Figure S1F). TNTs also contained microtubules [8,15] (illustrated by Actin or
98 Tubulin staining, Figure 1G and Figure S1G respectively), and mitochondria [16] (Mitotracker
99 green staining, Figure 1G; Figure S1H). Importantly, transformed cells could also establish TNT
100 connections with non-transformed primary epithelial mammary cells (Figure 1H) and
101 fibroblasts (Figure S1I), isolated from healthy human breast samples.
102 This indicates that early mammary cell transformation leads to an enhanced ability of
103 transformed cells to connect to their neighbors through TNTs.
104

105 **Directional transfer of cellular material *via* TNTs from transformed to non-transformed**
106 **cells.** To investigate how TNTs connect cells, we cocultured mCherry-expressing MCF10A-CT
107 with GFP-expressing M1B26 cells, seeded at low density [14]. Both M1B26 transformed (Tf) and
108 MCF10A-CT non-transformed (NoTf) cells formed TNT structures, connecting Tf to Tf, NoTf

to NoTf and Tf to NoTf cells (Figure 2A). Quantification of TNT contacts revealed that connections were more frequent and abundant from Tf towards NoTf cells than in the opposite direction (Figure 2B,C). Fluorescent material from GFP-tagged Tf cells accumulated within the cytoplasm of NoTf cells (Figure 2D), suggesting a directional transfer *via* TNTs, Tf cells as donors and NoTf cells as acceptors (Figure 2E; Movie S1; Figure S2A). To assess the proportion of cellular exchange between cells, mCherry-NoTf cells were cocultured with GFP-Tf cells for 8 days. Flow cytometry analysis revealed a higher proportion of mCherry-NoTf cells exhibiting green fluorescence uptake compared to GFP-Tf cells acquiring red fluorescence (Figure S2B), indicating a preferential Tf-to-NoTf directional transfer (Figure 2F-H). Switching fluorophores between Tf and NoTf cells yielded similar results (Figure S2C,D), and this directional transfer increased over time (Figure S2E-I). When using normal human primary mammary cells as NoTf cell sources, we also observed a Tf-to-NoTf directional material transfer in coculture (Figure 2J,K), as with MCF10A-CT cells (Figure S2J). To evaluate the contribution of cell-cell communication through secretion of soluble compounds and extracellular vesicles, we performed cultures of normal human primary cells with Tf cells separated by a physical barrier (Transwell™), to impede TNT formation or in the presence of Tf cells conditioned medium (CM, as illustrated in Figure 2I). In the former condition, the number of acceptor cells dropped in both transfer directions (Figure 2J,K; Figure S2J). In the latter, no fluorescence exchange *via* soluble components was observed (Figure S2K,L).

Therefore, directional material transfer preferentially occurs *via* TNTs from Tf to NoTf cells, and rather than through other forms of cell-cell communication.

TNT-mediated transfer modulates proteomic features of acceptor cells.

To investigate the molecular consequences of intercellular material transfer, we performed a proteomic analysis of distinct cell populations isolated from long-term cocultures. Fluorescently-labeled cells cultured for 8 days (Figure 3A), were sorted by flow cytometry into four populations: non-transformed (NoTf), transformed (Tf), non-transformed cells that received fluorescent material (NoTf accept), and non-transformed cells from the same coculture that did not receive any material (NoTf no accept). Unbiased proteomic screening of each population followed by gene enrichment pathway analysis revealed that most enriched pathways in NoTf accept, compared to NoTf no accept of the same coculture, were related to transport (organic/nitrogen compounds, protein, transmembrane, intracellular), and to localization of intracellular organelles, macromolecules and proteins (Figure 3B). Other

142 pathways pointed to mitochondrion organization and activity. Volcano plot analysis revealed
143 that NoTf accept were statistically distinct from NoTf no accept cells of the same coculture,
144 and from NoTf in monoculture (Figure 3C; Figure S3A). Of note, the most overexpressed
145 proteins in the former phenotype were involved in lipid metabolism and transport (*ATP8B1,*
146 *RAB6B, CES1/* EST1, *MEST*, *PIGA*), intracellular membrane and secretory vesicle trafficking
147 (*RAB6B, RAB11B, SYT8, CAV2, TMEM167A*), cell growth and morphology maintenance
148 (*TRIQK*), membrane protrusion formation (*ATP8B1*) and actin filament bundling (*LCP1*/
149 Plastin-2) (Table S1). Other overexpressed proteins were linked to mitochondrial activities
150 (*COX7C*, *MALSU1*), likely related to the presence of mitochondria within TNTs (Figure 1G;
151 Figures. S1H, S3B).
152 Six proteins, EST1, Plastin-2, Rab-6B, TRIQK, MEST and MASU1, were markedly
153 overexpressed in NoTf accept compared to NoTf no accept cells from same cocultures (Figure
154 3D; Figure S3C). Corresponding RNA levels were also enhanced in Tf compared to NoTf cells
155 (Figure S3D). The TNT-mediated transfer of material therefore induces in acceptor cells
156 transcriptional and translational upregulation of key actors of membrane, cytoskeleton and cell
157 homeostasis, while some others are downregulated, such as DAP1 (*DAP*) and thymosin β-10
158 (*TMSB10*), respectively involved in ribosome hibernation and actin polymerization inhibition
159 (Table S1).
160 When TNT formation was physically impeded, acceptor cells showed phenotypic differences
161 compared to those in direct coculture (Table S2), but remained comparable to NoTf cells in
162 monoculture (Figure S3E,F). Notably, NoTf accept cells from direct cocultures exhibited a
163 higher expression of early inflammatory markers (*SERPINA3, CD14*) and motility-related
164 genes (*IGFBP6*) than their Transwell™ counterparts. These findings indicate that TNT-
165 mediated direct contacts with transformed cells induce profound changes in the proteomic
166 landscape of non-transformed acceptor cells, similar to those observed in early transformed
167 cells (M1B26 cells).
168 Ras-driven oncogenic transformation being a well-established process, we next investigated
169 whether it could also be impacted by the formation of TNTs. Proteomics revealed a marked
170 increase in H-Ras and K-Ras oncoproteins in NoTf accept cells compared to NoTf cells in
171 monoculture (Figure 3E). We next evaluated whether Ras-driven transformation influences
172 TNT formation in mammary cells using two additional models of Ras-mediated transformation
173 of mammary epithelial cells. First, in the Weinberg's model of human mammary epithelial cells
174 immortalized with SV40-L antigen and hTERT, then transformed with H-Ras [17], TNTs were
175 present in malignant and non-malignant cells, with shorter TNTs in the former (Figure 3F,H).

176 Second, in H-Ras-transformed immature MCF10A-derived AT1 and DCIS cells, malignant
177 cells exhibited fewer TNTs than non-malignant ones, without length difference (Figure 3G,I).
178 Hence, Ras-induced transformation does not enhance long-distance TNT-mediated
179 communication, contrary to inflammation- and BMP-driven mechanisms relevant to luminal
180 breast cancer clinical occurrence [3,18].
181
182 **TNT-mediated transfer impacts the BMP pathway of recipient cells.**
183 Since transmembrane and protein transports were the most impacted processes (Figure 3B), and
184 given that the BMP pathway is involved in luminal transformation [3,4] (Figure S4A,B), we
185 examined whether this pathway was affected in non-transformed acceptor cells. We focused on
186 the canonical SMAD cascade, and among non-canonical MAPK downstream cascades, on p38
187 (MAPK14), because the p-p38/p38 ratio exhibited the highest level of expression in Tf cells
188 (Figure S4A,B). This choice is further supported by the established role of p38 MAPK as a key
189 regulator of oncogenic stress responses and transformation in mammary epithelial cells. Eight
190 target or regulator proteins of these cascades were extracted from our proteomic screening
191 (Table S3), and assessed for their expression across sorted cell populations post-TNT
192 connections (Figure 3A). Several proteins involved in the BMP pathway, including ID1,
193 Nup214 [19], spartin, and USP15 [20], were consistently up- or down-regulated in NoTf acceptor
194 cells, reaching levels comparable to those observed in Tf cells (M1B26), exclusively after TNT
195 transfer (Figure 4A). ATF2, a transcription regulator positioned at the BMP pathway/p38
196 cascade interface, was under-expressed in NoTf acceptor cells, at levels comparable to those in
197 Tf cells. Components of the p38 cascade were markedly altered following TNT-mediated
198 transfer: MAPKAPK2, a kinase activated by p38 phosphorylation, was under-expressed in
199 NoTf acceptor cells, consistent with the role of p38 inhibition in facilitating mammary
200 tumorigenesis [21]. Conversely Rac1, part of a complex involved in actin bundling and
201 stabilization, regulated by p38, was overexpressed in NoTf cells that received material *via* TNTs
202 (Figure 4A). At the level of the BMP signaling elements, BMPR1b was localized within TNTs,
203 particularly in bulges, in normal human primary and model mammary cells (Figure 4B).
204 Correlative light (scanning) electron microscopy (CLEM) enables to distinguish intra- from
205 extra-cellular epitopes by overlaying optical and scanning electron images of the same region.
206 Airyscan confocal imaging revealed a continuum of BMPR1b in cell bodies, as well as in or on
207 TNTs. However, electron microscopy did not reveal any extracellular BMPR1b epitopes at
208 TNTs (Figure 4C). This suggests an extracellular localization in the cell body and an
209 intraluminal presence in TNTs, consistent with BMPR1b trafficking through/within TNTs.

210 Although incomplete (Figure 4D,E top), *BMPR1b* silencing in Tf cells drastically reduced TNT
211 number, and abolished the formation of long TNTs (Figure 4E bottom). Silencing of G protein-
212 coupled estrogen receptor 1 (*GPER*) was used as control, since no report linked GPER to TNT
213 formation/function. Though more efficient than *BMPR1b* silencing (Figure 4E top), *GPER*
214 knockdown had no effect on TNT number or length (Figure 4D,E bottom). Therefore, BMPR1b
215 contributes to the formation and elongation of (long) TNTs.
216 The four sorted cell populations (Figures 3A, 4F) were then analyzed for BMPR1b mRNA
217 expression. It was found ~8-fold higher in NoTf accept cells previously connected *via* TNTs,
218 compared to an only ~2-fold increase when TNT formation was blocked (Figure 4G). This
219 supports a role for a TNT-mediated activation of the BMP pathway.
220 Together, these findings indicate that TNT-mediated material transfer from Tf cells remodels
221 signaling components in recipient NoTf cells, including increased BMPR1b expression, and
222 identify BMPR1b as a specific regulator of TNT formation.
223
224 **After TNT contact with transformed donor cells, non-transformed acceptor cells become**
225 **sensitized to a transforming microenvironment.**
226 Long-term impact of TNT cell-cell communication was assessed on sorted cells, cultured for
227 up to 16 weeks in the absence or presence BMP2/IL6, mimicking *in vivo* luminal breast tumor
228 conditions [3,18] (Figure 4F). BMPR1b protein levels rose between weeks 6 and 10 before
229 stabilizing, in NoTf accept cells exposed to cytokines after sorting (Fig. 5A left), reaching the
230 highest expression among all populations by week 14 (Figure 5A right; Figure S4C,D). In the
231 tumor model designed in our laboratory, recapitulating the clinical relevance of early steps of
232 luminal breast tumor initiation and progression [3,5] (Figure 1A), enhanced BMPR1b expression
233 correlated with the activation of canonical BMP signaling, as evidenced by SMAD1/5/8
234 phosphorylation, and non-canonical MAPK cascades, including p-p38/p38 and p-ERK/ERK
235 (Figure S4A,B). After an 8-day TNT contact with Tf cells, followed by sorting and re-culture,
236 NoTf accept cells displayed activation of the p-SMAD1/5/8 / SMAD1/5/8 and p-p38/p38
237 cascades, upon a 4 to 6 week-exposure to BMP2/IL6 (Figure 5B,C; Figure S4E,F). While the
238 SMAD cascade did not return to baseline over weeks (Figure 5B), the p38 cascade, after a
239 strong activation as early as 4 weeks with cytokines post-sorting, reached baseline levels after
240 10 weeks (Figure 5C).
241 We then cross-referenced our proteomic and transcriptomic datasets [5], and identified three
242 tumor-associated genes significantly upregulated during transformation: *HOXB6* [22], *CCND2* [23],
243 and *EREG* [24] (Figure 5D). Their mRNA levels were increased in NoTf acceptor cells connected

through TNTs with Tf cells, compared to NoTf cells in monoculture, and to NoTf acceptor cells for which TNT formation was blocked (Figure 5E). This supports the notion that TNT-mediated transfer may promote a shift towards a preneoplastic state. HoxB6, Cyclin D2 and (pro)-epiregulin protein levels also tended to increase with transformation (Figure S5A). *HRAS* was overexpressed in NoTf acceptor cells, further substantiating a shift towards a preneoplastic status (Figure 4E). However, *HRAS* was neither involved in TNT formation, nor in TNT-mediated preneoplastic switch of acceptor cells (Figure 3F-I). As a negative control, we selected *UFM1*, a gene involved in endoplasmic reticulum stress, a cellular insult suggested to contribute to TNT development [25]. *UFM1* transcript levels remained unchanged regardless of transformation status or material uptake (Figure S5B,C), indicating that although ER stress may be present, it is not a key driver of the cellular behavior described here.

NoTf acceptor cells grown in the presence of the pro-transforming cytokines BMP2 and IL6 [3,5] up to 16 weeks post-TNT transfer and sorting (Figure S6A), displayed anchorage-independent growth at earlier time points than other types of sorted cells, and with a number of clones obtained comparable to that of Tf cells (Figure 5F; Figure S6B). Potential cross-contamination between Tf and NoTf sorted cell samples was ruled out based on the specific fluorescence of derived soft agar clones (Figure S6C). All these features are hallmarks of a preneoplastic transformation, observed exclusively in cells that had established TNT contacts with transformed cells prior to sorting, enabling the transfer of transforming information.

Hence, these findings unravel the key role of TNT-mediated transfer of transforming cues, including BMPR1b, in driving a preneoplastic switch in previously non-transformed cells receiving material from transformed cells. This TNT communication would prime non-transformed cells to respond to a tumor-promoting microenvironment, ultimately contributing to the propagation of transformation (Figure 5G).

Discussion

Tunneling nanotubes (TNTs) have been extensively implicated in cancer progression through the intercellular transfer of mitochondria, notably from stromal cells to cancer (stem) cells [26], and more recently from neurons to cancer cells to enhance metastatic capacity [10]. Building on this framework, our findings reveal that TNT-mediated transfer of transforming cues from transformed to non-transformed cells activates BMP signaling in recipient cells, concomitant with increased BMPR1b expression, thereby sensitizing them to a tumor-promoting microenvironment and promoting the early acquisition of preneoplastic features.

In contrast, the delivery of material from transformed cells to non-transformed neighbors, remains unexplored at very early stages of transformation. Our study is the first to investigate the functional impact of TNT-mediated material exchange between cells of identical phenotype (i.e. epithelial cells), on the predisposition of non-transformed cells to adopt a preneoplastic status. Although donor-to-acceptor material transfer through secretion of soluble compounds and extracellular vesicles occurred, it remained low to negligible, indicating that the processes mainly relied on physical TNT-mediated communications. This directional transfer from transformed to non-transformed cells leads within days to the overexpression of tumor-related genes and of BMPR1b itself, evocative of a possible feedback loop that maintains transforming conditions (Figure 5G). Non-transformed cells also undergo profound changes of their proteomic landscape, linked to transport processes, and within weeks acquire phenotypic traits of preneoplasia, such as anchorage-independent growth, sustained BMPR1b overamplification and related mounting of a non-canonical signaling cascade. The earliest events, within one week, comprised the overexpression of tumor-related genes such as *HOXB6*, *CCND2* and *EREG* by non-transformed acceptor cells, after TNT contacts with transformed (donor) cells. Interestingly, upregulation of these genes upon transformation has already been linked to other cancers: (i) *HOXB6*, encoding a homeobox domain-containing transcription factor involved in development, is upregulated in acute myeloid leukemia and osteosarcoma [22,27], with a possible role in cancer initiation [28]; (ii) *CCND2*, encoding cyclin D2, involved in DNA replication, cell division and cell cycle regulation, was dysregulated in gastric, thyroid and colorectal cancers [29], and its overexpression in breast cancer promotes MAPK-mediated cell proliferation and tumor growth [23,30]; (iii) upregulation of *EREG,* encoding the secreted protein ligand of the EGF receptor (EGFR) epiregulin, is linked to breast cancer progression and resistance to tamoxifen by EGFR activation [24,31]. Interestingly, experiments on TNT-forming capacities of mammary cell models, where transformation of either normal primary [17] or MCF10A cells [32] is « switched

302 on » by the H-Ras oncoprotein, showed fewer and shorter TNTs connecting cells. *HRAS* is
303 overexpressed in invasive breast tumors, but the prevalence of *HRAS* mutations in luminal types
304 is negligible [1,33]. These mammary models do not faithfully recapitulate the earliest stages of
305 non-invasive luminal breast tumors triggered, for example, by exposure to carcinogenic cues
306 such as environmental pollutants, endocrine disruptors or alcohol [3,34–36].

307 Following TNT material transfer, including BMPR1b, *BMPR1B* becomes overexpressed in
308 acceptor cells within a week. The receptor molecule was detected within TNTs, overexpressed
309 in transformed cells, and structurally contributing to TNT elongation. As BMP receptors are
310 known to be located in lipid rafts, BMPR1b could induce TNT formation *via* its interaction with
311 these microdomains [37], from which TNTs might arise [38,39]. These cholesterol-rich microdomains
312 provide high curvature and elasticity necessary for membrane deformation linked to TNT
313 formation. Cholesterol levels together with lipid rafts increase upon transformation, as
314 evidenced in prostate and breast cancer cell lines [40], further substantiated by our proteomic data
315 with acceptor cells displaying enhanced expression of EST1, a carboxylesterase hydrolyzing
316 cholesterol esters into free cholesterol. Additionally, BMP2 was reported to promote actin
317 polymerization via PI3Kα activation [41]. We herein observed that *LCP1* was upregulated upon
318 transformation, concomitantly to its protein Plastin-2, in acceptor cells following TNT transfer.
319 Plastin-2 is a key actin-bundling protein involved in the formation of cellular protrusions [42],
320 overexpressed in epithelial-derived cancers including breast [43]. Its overexpression correlated
321 with cancer cell migration, invasion, metastasis [44] and chemoresistance [45]. Plastin-2 activation
322 depends on serine 5 phosphorylation *via* ERK/MAPK, PI3K, and PKA/PKC pathways,
323 enabling its recruitment to actin filaments and promoting bundling and protrusion elongation,
324 as shown in breast carcinoma [46]. This agrees with findings from the Zurzolo's group, showing
325 that TNT induction by Eps8 involves its actin-bundling activity [47]. Altogether, this might
326 explain the higher number of TNTs observed upon transformation.

327 At the functional level, the analysis of sorted acceptor cells which received material from TNT
328 transfer, revealed their gradual transformation over weeks, faster and more extensively than
329 non-acceptor cells, concomitant to a progressive but sustained activation of the BMP pathway.
330 This induced an initial burst of p38 downstream response, followed by the prolonged activation
331 of the canonical SMAD cascade, only observed when TNT contacts existed. The p38 MAPK
332 pathway is a well-established regulator of mammary epithelial cell transformation, acting as an
333 early stress-responsive barrier through the induction of cell-cycle arrest, oncogene-induced
334 senescence, and apoptosis [48], while being frequently bypassed or reprogrammed during tumor

335 progression to support cellular plasticity [49]. Beyond its role in stress signaling, p38 also
336 regulates cytoskeletal dynamics, lamellipodium formation and cell migration [41,50]. Consistent
337 with this framework, our data indicate that TNT-mediated material transfer triggers a rapid
338 activation of the p38 pathway, which is subsequently efficiently repressed, thereby enabling the
339 emergence of preneoplastic traits in recipient cells.

340 Here, we unveil for the first time that TNTs transport BMPR1b and propagate transforming
341 cues, in the context of luminal breast cancer initiation. Such processes sensitize acceptor cells
342 to BMP2 signals of the microenvironment, rapidly triggering a cascade of molecular events that
343 culminate in phenotypic changes, with anchorage-independent growth of previously non-
344 transformed cells (Figure 5F-G). Combined with the recent demonstration that TNTs can
345 transfer material *in vivo* [51], our work provides the foundation for a new concept: the
346 propagation, through TNTs, of a preneoplastic state within a population of initially non-
347 transformed mammary cells. This process could precede the development of luminal-type
348 tumors, and identify BMPR1b as a major early contributor of the BMP-dependent preneoplastic
349 switch of acceptor cells.

350

Data availability statement. The mass spectrometry proteomics data have been deposited to the ProteomeXchange Consortium via the PRIDE (https://www.ebi.ac.uk/pride/) [52,53] partner repository, with the dataset identifier PXD060023. Transcriptomic data have been deposited on the Gene Expression Omnibus repository, GSE18673411.

Acknowledgements. We thank P. Battiston-Montagne, M. Gautier and C. Vanbelle (CRCL, platform PIC), and D. Ressnikoff (SFR Santé Lyon Est, CIQLE). We thank the "AniRA lentivectors production facility" from the CELPHEDIA Infrastructure and SFR Biosciences, UAR3444/CNRS, US8/Inserm, ENS de Lyon, UCBL, especially G. Froment, D. Nègre and C. Costa. We thank J. Brocard, head of the LYMIC-PLATIM UAR 3444 / US8 microscopy platform (ENS Lyon, Univ Lyon 1), and E. Chatre. We thank B. Manship for english proofreading, P. Mehlen, P. Juin, R. Tomasini, C. Vérollet and B. Bartosch for inspiring discussions. Some illustrations were created in https://BioRender.com.
This work was supported by Agence Nationale de la Recherche (VMS, ANR-10-LABX-0061, ANR-CESA-018-04 and Convergence PLAsCAN ANR-17-CONV-0002); Ligue Nationale contre le Cancer (CCM, doctoral grant), Dept Ain, Rhône (VMS), Saône et Loire (EIP) ; Fondation ARC (CCM, 4th year doctoral grant; VMS, SFI20111203500, PJA20171206331) ; the ERiCAN program of Fondation MSD-Avenir (VMS/EIP, DS-2018-0015) and Associations [Déchaîne Ton Cœur (VMS); Ruban Rose Prix Avenir 2021 (VMS) ; Comité féminin pour le dépistage du cancer du sein 74 (VMS) ; Symatese Fondation (VMS), and Fondation pour la Recherche Médicale (équipe FRM EQU202203014695 VMS).

Contributions: V.M.S. and E-I.P designed and supervised the study, conceived methodological developments and acquired funding. V.M.S. provided administrative support. C.C.M., S.L. and B.G. collaborated in study design, contributed to methodological developments and data interpretations. K.G. performed RNA-seq and proteomic bioinformatic data analyses, and statistical gene-expression analyses. C.C.M., T.T.N., A.B. and E-I.P. performed and interpreted the experiments. C.D. designed and performed SEM and CLEM microscopy experiments. F.G., A.B. and C.H. performed proteomic analyses, and F.G. interpreted proteomic data. E.D. provided primary breast samples, and assisted with their processing. C.C.M., V.M.S and E-I.P. wrote the manuscript. All authors reviewed the manuscript and approved the final version for publication.

Competing interests. The authors declare no competing interests.

References.

1. Cancer Genome Atlas Network (2012). Comprehensive molecular portraits of human breast tumors. Nature *490*, 61–70. https://doi.org/10.1038/nature11412.

2. Zabala, M., Lobo, N.A., Antony, J., Heitink, L.S., Gulati, G.S., Lam, J., Parashurama, N., Sanchez, K., Adorno, M., Sikandar, S.S., et al. (2020). LEFTY1 Is a Dual-SMAD Inhibitor that Promotes Mammary Progenitor Growth and Tumorigenesis. Cell Stem Cell *27*, 284-299.e8. https://doi.org/10.1016/j.stem.2020.06.017.

3. Chapellier, M., Bachelard-Cascales, E., Schmidt, X., Clément, F., Treilleux, I., Delay, E., Jammot, A., Ménétrier-Caux, C., Pochon, G., Besançon, R., et al. (2015). Disequilibrium of BMP2 levels in the breast stem cell niche launches epithelial transformation by overamplifying BMPR1B cell response. Stem Cell Rep. *4*, 239–254. https://doi.org/10.1016/j.stemcr.2014.12.007.

4. Jiang, W.-J., Zhou, T.-H., Huang, H.-J., Li, L.-S., Tan, H., Zhang, R., Wang, Q.-S., and Feng, Y.-M. (2025). Breast Cancer Subtype–Specific Organotropism Is Dictated by FOXF2-Regulated Metastatic Dormancy and Recovery. Cancer Res. *85*, 644–659. https://doi.org/10.1158/0008-5472.CAN-24-0479.

5. Guyot, B., Clément, F., Drouet, Y., Schmidt, X., Lefort, S., Delay, E., Treilleux, I., Foy, J.-P., Jeanpierre, S., Thomas, E., et al. (2023). An Early Neoplasia Index (ENI10), Based on Molecular Identity of CD10 Cells and Associated Stemness Biomarkers, is a Predictor of Patient Outcome in Many Cancers. Cancer Res. Commun. *3*, 1966–1980. https://doi.org/10.1158/2767-9764.CRC-23-0196.

6. Ju, F., Atyah, M.M., Horstmann, N., Gul, S., Vago, R., Bruns, C.J., Zhao, Y., Dong, Q.-Z., and Ren, N. (2022). Characteristics of the cancer stem cell niche and therapeutic strategies. Stem Cell Res. Ther. *13*, 233. https://doi.org/10.1186/s13287-022-02904-1.

7. Bayik, D., and Lathia, J.D. (2021). Cancer stem cell-immune cell crosstalk in tumour progression. Nat. Rev. Cancer *21*, 526–536. https://doi.org/10.1038/s41568-021-00366-w.

8. Resnik, N., Erman, A., Veranič, P., and Kreft, M.E. (2019). Triple labelling of actin filaments, intermediate filaments and microtubules for broad application in cell biology: uncovering the cytoskeletal composition in tunneling nanotubes. Histochem. Cell Biol. *152*, 311–317. https://doi.org/10.1007/s00418-019-01806-3.

9. Rustom, A., Saffrich, R., Markovic, I., Walther, P., and Gerdes, H.-H. (2004). Nanotubular highways for intercellular organelle transport. Science *303*, 1007–1010. https://doi.org/10.1126/science.1093133.

10. Hoover, G., Gilbert, S., Curley, O., Obellianne, C., Lin, M.T., Hixson, W., Pierce, T.W., Andrews, J.F., Alexeyev, M.F., Ding, Y., et al. (2025). Nerve-to-cancer transfer of mitochondria during cancer metastasis. Nature *644*, 252–262. https://doi.org/10.1038/s41586-025-09176-8.

11. Pinto, G., Brou, C., and Zurzolo, C. (2020). Tunneling Nanotubes: The Fuel of Tumor Progression? Trends Cancer *6*, 874–888. https://doi.org/10.1016/j.trecan.2020.04.012.

12. Vignais, M.-L., Caicedo, A., Brondello, J.-M., and Jorgensen, C. (2017). Cell Connections by Tunneling Nanotubes: Effects of Mitochondrial Trafficking on Target Cell Metabolism, Homeostasis, and Response to Therapy. Stem Cells Int. *2017*, 6917941. https://doi.org/10.1155/2017/6917941.

13. Huang, L., Zhang, J., Wu, Z., Zhou, L., Yu, B., Jing, Y., Lin, D., and Qu, J. (2022). Revealing the structure and organization of intercellular tunneling nanotubes (TNTs) by STORM imaging. Nanoscale Adv. *4*, 4258–4262. https://doi.org/10.1039/d2na00415a.

14. Sáenz-de-Santa-María, I., Henderson, J.M., Pepe, A., and Zurzolo, C. (2023). Identification and Characterization of Tunneling Nanotubes for Intercellular Trafficking. Curr. Protoc. *3*, e939. https://doi.org/10.1002/cpz1.939.

15. Cordero Cervantes, D., and Zurzolo, C. (2021). Peering into tunneling nanotubes-The path forward. EMBO J. *40*, e105789. https://doi.org/10.15252/embj.2020105789.

16. Pinto, G., Saenz-de-Santa-Maria, I., Chastagner, P., Perthame, E., Delmas, C., Toulas, C., Moyal-Jonathan-Cohen, E., Brou, C., and Zurzolo, C. (2021). Patient-derived glioblastoma stem cells transfer mitochondria through tunneling nanotubes in tumor organoids. Biochem. J. *478*, 21–39. https://doi.org/10.1042/BCJ20200710.

17. Elenbaas, B., Spirio, L., Koerner, F., Fleming, M.D., Zimonjic, D.B., Donaher, J.L., Popescu, N.C., Hahn, W.C., and Weinberg, R.A. (2001). Human breast cancer cells generated by oncogenic transformation of primary mammary epithelial cells. Genes Dev. *15*, 50–65. https://doi.org/10.1101/gad.828901.

18. Iliopoulos, D., Hirsch, H.A., Wang, G., and Struhl, K. (2011). Inducible formation of breast cancer stem cells and their dynamic equilibrium with non-stem cancer cells via IL6 secretion. Proc. Natl. Acad. Sci. U. S. A. *108*, 1397–1402. https://doi.org/10.1073/pnas.1018898108.

19. Sapkota, G., Alarcón, C., Spagnoli, F.M., Brivanlou, A.H., and Massagué, J. (2007). Balancing BMP signaling through integrated inputs into the Smad1 linker. Mol. Cell *25*, 441–454. https://doi.org/10.1016/j.molcel.2007.01.006.

20. Inui, M., Manfrin, A., Mamidi, A., Martello, G., Morsut, L., Soligo, S., Enzo, E., Moro, S., Polo, S., Dupont, S., et al. (2011). USP15 is a deubiquitylating enzyme for receptor-activated SMADs. Nat. Cell Biol. *13*, 1368–1375. https://doi.org/10.1038/ncb2346.

21. Wen, H.-C., Avivar-Valderas, A., Sosa, M.S., Girnius, N., Farias, E.F., Davis, R.J., and Aguirre-Ghiso, J.A. (2011). p38α Signaling Induces Anoikis and Lumen Formation During Mammary Morphogenesis. Sci. Signal. *4*, ra34. https://doi.org/10.1126/scisignal.2001684.

22. Fischbach, N.A., Rozenfeld, S., Shen, W., Fong, S., Chrobak, D., Ginzinger, D., Kogan, S.C., Radhakrishnan, A., Le Beau, M.M., Largman, C., et al. (2005). HOXB6 overexpression in murine bone marrow immortalizes a myelomonocytic precursor in vitro and causes hematopoietic stem cell expansion and acute myeloid leukemia in vivo. Blood *105*, 1456–1466. https://doi.org/10.1182/blood-2004-04-1583.

23. Ouyang, J., Liu, Z., Yuan, X., Long, C., Chen, X., Wang, Y., Liu, L., Liu, S., and Liang, H. (2021). LncRNA PRNCR1 Promotes Breast Cancer Proliferation and Inhibits Apoptosis by Modulating microRNA-377/CCND2/MEK/MAPK Axis. Arch. Med. Res. *52*, 471–482. https://doi.org/10.1016/j.arcmed.2021.01.007.

24. He, M., Jin, Q., Chen, C., Liu, Y., Ye, X., Jiang, Y., Ji, F., Qian, H., Gan, D., Yue, S., et al. (2019). The miR-186-3p/EREG axis orchestrates tamoxifen resistance and aerobic glycolysis in breast cancer cells. Oncogene *38*, 5551–5565. https://doi.org/10.1038/s41388-019-0817-3.

25. Wang, Y., Cui, J., Sun, X., and Zhang, Y. (2011). Tunneling-nanotube development in astrocytes depends on p53 activation. Cell Death Differ. *18*, 732–742. https://doi.org/10.1038/cdd.2010.147.

26. Nakhle, J., Khattar, K., Özkan, T., Boughlita, A., Abba Moussa, D., Darlix, A., Lorcy, F., Rigau, V., Bauchet, L., Gerbal-Chaloin, S., et al. (2023). Mitochondria Transfer from Mesenchymal Stem Cells Confers Chemoresistance to Glioblastoma Stem Cells through Metabolic Rewiring. Cancer Res. Commun. *3*, 1041–1056. https://doi.org/10.1158/2767-9764.CRC-23-0144.

27. Huang, H., Lu, D., Li, K., Zheng, M., Qin, X., Cui, X., Chen, Y., Chen, C., Huang, N., Zheng, L., et al. (2023). Hsa_circ_0007031 promotes the proliferation and migration of osteosarcoma cells by sponging miR-196a-5p to regulate the HOXB6. Biochem. Pharmacol. *214*, 115667. https://doi.org/10.1016/j.bcp.2023.115667.

28. Vider, B.Z., Zimber, A., Chastre, E., Gespach, C., Halperin, M., Mashiah, P., Yaniv, A., and Gazit, A. (2000). Deregulated expression of homeobox-containing genes, HOXB6, B8, C8, C9, and Cdx-1, in human colon cancer cell lines. Biochem. Biophys. Res. Commun. *272*, 513–518. https://doi.org/10.1006/bbrc.2000.2804.

29. Ding, Z.-Y., Li, R., Zhang, Q.-J., Wang, Y., Jiang, Y., Meng, Q.-Y., Xi, Q.-L., and Wu, G.-H. (2019). Prognostic role of cyclin D2/D3 in multiple human malignant neoplasms: A systematic review and meta-analysis. Cancer Med. *8*, 2717–2729. https://doi.org/10.1002/cam4.2152.

30. Zhong, H., Yang, J., Zhang, B., Wang, X., Pei, L., Zhang, L., Lin, Z., Wang, Y., and Wang, C. (2018). LncRNA GACAT3 predicts poor prognosis and promotes cell proliferation in breast cancer through regulation of miR-497/CCND2. Cancer Biomark. Sect. Dis. Markers *22*, 787–797. https://doi.org/10.3233/CBM-181354.

31. Abba, M.C., Canzoneri, R., Gurruchaga, A., Lee, J., Tatineni, P., Kil, H., Lacunza, E., and Aldaz, C.M. (2020). LINC00885 a Novel Oncogenic Long Non-Coding RNA Associated with Early Stage Breast Cancer Progression. Int. J. Mol. Sci. *21*, 7407. https://doi.org/10.3390/ijms21197407.

32. Dawson, P.J., Wolman, S.R., Tait, L., Heppner, G.H., and Miller, F.R. (1996). MCF10AT: a model for the evolution of cancer from proliferative breast disease. Am. J. Pathol. *148*, 313–319.

33. Kim, S.-J., Saeidi, S., Cho, N.-C., Lee, H.-B., Han, W., Kim, K.P., and Surh, Y.-J. (2025). Cooperation between oncogenic NRF2 and wild-type HRAS promotes progression of breast cancer. Cell. Signal. *134*, 111920. https://doi.org/10.1016/j.cellsig.2025.111920.

34. Romieu, I., Scoccianti, C., Chajès, V., de Batlle, J., Biessy, C., Dossus, L., Baglietto, L., Clavel-Chapelon, F., Overvad, K., Olsen, A., et al. (2015). Alcohol intake and breast cancer in the European prospective investigation into cancer and nutrition. Int. J. Cancer *137*, 1921–1930. https://doi.org/10.1002/ijc.29469.

35. Giampiccolo, C., Fervers, B., Coudon, T., Praud, D., Vigneron, A., Grassot, L., Mercoeur, B., Faure, E., Frenoy, P., Génard-Walton, M., et al. (2026). Statistical approaches to analyse the combined effect of seven air pollutants and breast cancer risk: a case–control study nested in the French E3N-Generations cohort. BMC Med. *24*, 112. https://doi.org/10.1186/s12916-026-04653-x.

36. Clément, F., Xu, X., Donini, C.F., Clément, A., Omarjee, S., Delay, E., Treilleux, I., Fervers, B., Le Romancer, M., Cohen, P.A., et al. (2017). Long-term exposure to bisphenol A or benzo(a)pyrene alters the fate of human mammary epithelial stem cells in response to BMP2 and BMP4, by pre-activating BMP signaling. Cell Death Differ. *24*, 155–166. https://doi.org/10.1038/cdd.2016.107.

37. Hirschhorn, T., Levi-Hofman, M., Danziger, O., Smorodinsky, N.I., and Ehrlich, M. (2017). Differential molecular regulation of processing and membrane expression of Type-I BMP receptors: implications for signaling. Cell. Mol. Life Sci. CMLS *74*, 2645–2662. https://doi.org/10.1007/s00018-017-2488-y.

38. Reindl, J., Shevtsov, M., Dollinger, G., Stangl, S., and Multhoff, G. (2019). Membrane Hsp70-supported cell-to-cell connections via tunneling nanotubes revealed by live-cell STED nanoscopy. Cell Stress Chaperones *24*, 213–221. https://doi.org/10.1007/s12192-018-00958-w.

39. Thayanithy, V., Babatunde, V., Dickson, E.L., Wong, P., Oh, S., Ke, X., Barlas, A., Fujisawa, S., Romin, Y., Moreira, A.L., et al. (2014). Tumor exosomes induce tunneling nanotubes in lipid raft-enriched regions of human mesothelioma cells. Exp. Cell Res. *323*, 178–188. https://doi.org/10.1016/j.yexcr.2014.01.014.

40. Li, Y.C., Park, M.J., Ye, S.-K., Kim, C.-W., and Kim, Y.-N. (2006). Elevated levels of cholesterol-rich lipid rafts in cancer cells are correlated with apoptosis sensitivity induced by cholesterol-depleting agents. Am. J. Pathol. *168*, 1107–1118; quiz 1404–1405. https://doi.org/10.2353/ajpath.2006.050959.

41. Gamell, C., Osses, N., Bartrons, R., Rückle, T., Camps, M., Rosa, J.L., and Ventura, F. (2008). BMP2 induction of actin cytoskeleton reorganization and cell migration requires PI3-kinase and Cdc42 activity. J. Cell Sci. *121*, 3960–3970. https://doi.org/10.1242/jcs.031286.

42. Ishida, H., Jensen, K.V., Woodman, A.G., Hyndman, M.E., and Vogel, H.J. (2017). The Calcium-Dependent Switch Helix of L-Plastin Regulates Actin Bundling. Sci. Rep. *7*, 40662. https://doi.org/10.1038/srep40662.

43. Lin, C.S., Park, T., Chen, Z.P., and Leavitt, J. (1993). Human plastin genes. Comparative gene structure, chromosome location, and differential expression in normal and neoplastic cells. J. Biol. Chem. *268*, 2781–2792.

44. Riplinger, S.M., Wabnitz, G.H., Kirchgessner, H., Jahraus, B., Lasitschka, F., Schulte, B., van der Pluijm, G., van der Horst, G., Hämmerling, G.J., Nakchbandi, I., et al. (2014). Metastasis of prostate cancer and melanoma cells in a preclinical in vivo mouse model is enhanced by L-plastin expression and phosphorylation. Mol. Cancer *13*, 10. https://doi.org/10.1186/1476-4598-13-10.

45. Janji, B., Vallar, L., Al Tanoury, Z., Bernardin, F., Vetter, G., Schaffner-Reckinger, E., Berchem, G., Friederich, E., and Chouaib, S. (2010). The actin filament cross-linker L-plastin confers resistance to TNF-alpha in MCF-7 breast cancer cells in a phosphorylation-dependent manner. J. Cell. Mol. Med. *14*, 1264–1275. https://doi.org/10.1111/j.1582-4934.2009.00918.x.

46. Machado, R.A.C., Stojevski, D., De Landtsheer, S., Lucarelli, P., Baron, A., Sauter, T., and Schaffner-Reckinger, E. (2021). L-plastin Ser5 phosphorylation is modulated by the PI3K/SGK pathway and promotes breast cancer cell invasiveness. Cell Commun. Signal. CCS *19*, 22. https://doi.org/10.1186/s12964-021-00710-5.

47. Delage, E., Cervantes, D.C., Pénard, E., Schmitt, C., Syan, S., Disanza, A., Scita, G., and Zurzolo, C. (2016). Differential identity of Filopodia and Tunneling Nanotubes revealed by the opposite functions of actin regulatory complexes. Sci. Rep. *6*, 39632. https://doi.org/10.1038/srep39632.

48. Huot, J., Houle, F., Rousseau, S., Deschesnes, R.G., Shah, G.M., and Landry, J. (1998). SAPK2/p38-dependent F-actin reorganization regulates early membrane blebbing during stress-induced apoptosis. J. Cell Biol. *143*, 1361–1373. https://doi.org/10.1083/jcb.143.5.1361.

49. Llanses Martinez, Montserrat, Nan, Keqian, Bao, Zhe, Bacchetti, Rachele, Yuan, Shengnan, Tyler, Joe, Le Guezennec, Xavier, Bard, Frédéric A., and Rainero, Elena (2024). Novel kinase regulators of extracellular matrix internalisation identified by high-content screening modulate invasive carcinoma cell migration. PLoS Biol. *22*, e3002930. https://doi.org/doi:%252010.1371/journal.pbio.3002930.

554 50. Pichon, S., Bryckaert, M., and Berrou, E. (2004). Control of actin dynamics by p38 MAP kinase –
555 Hsp27 distribution in the lamellipodium of smooth muscle cells. J. Cell Sci. *117*, 2569–2577.
556 https://doi.org/10.1242/jcs.01110.

557 51. Korenkova, O., Liu, S., Prlesi, I., Pepe, A., Albadri, S., Del Bene, F., and Zurzolo, C. (2024).
558 Tunneling nanotubes enable intercellular transfer in zebrafish embryos. Dev. Cell, S1534-
559 5807(24)00635-X. https://doi.org/10.1016/j.devcel.2024.10.016.

560 52. Perez-Riverol, Y., Xu, Q.-W., Wang, R., Uszkoreit, J., Griss, J., Sanchez, A., Reisinger, F., Csordas,
561 A., Ternent, T., Del-Toro, N., et al. (2016). PRIDE Inspector Toolsuite: Moving Toward a Universal
562 Visualization Tool for Proteomics Data Standard Formats and Quality Assessment of
563 ProteomeXchange Datasets. Mol. Cell. Proteomics MCP *15*, 305–317.
564 https://doi.org/10.1074/mcp.O115.050229.

565 53. Perez-Riverol, Y., Bandla, C., Kundu, D.J., Kamatchinathan, S., Bai, J., Hewapathirana, S., John,
566 N.S., Prakash, A., Walzer, M., Wang, S., et al. (2025). The PRIDE database at 20 years: 2025 update.
567 Nucleic Acids Res. *53*, D543–D553. https://doi.org/10.1093/nar/gkae1011.

568

569

570 **Figure Legends.**

571 **Figure 1** | Structural characterization of TNTs upon mammary cell transformation. A,
572 Schematic of our MCF10A-derived cell lines *(5)*. B, Immunofluorescence images of actin (red)
573 in TNTs, observed by super-resolution Airyscan confocal microscopy with 40x oil objective.
574 Nuclei, Hoechst labeling (blue). Scale bars, 20 µm. C, TNT number (> 8 µm) quantification *per*
575 100 cells (left, n = 9 biological replicates), and % of long TNTs (> 50 µm; right, n = 4 biological
576 replicates). Ten Z-stacks of 10 sections each were taken *per* condition, and 100 cells minimum
577 *per* experiment were counted. TNTs were counted and measured in each Z-stack. Error bars
578 depict SD. P-values were calculated with one-way ANOVA with post-hoc Tukey test (ns, not
579 significant; * $p < 0.05$; ** $p < 0.01$; *** $p < 0.001$). D, Scanning electron microscopy images
580 of TNTs of MCF10A-CT, MC26 and M1B26 cells. Black arrow, TNT bulge. Scale bars
581 MCF10A-CT: 40 and 50 µm; MC26: 50 and 5 µm; M1B26: from left to right: 20, 3, 20, 3 µm.
582 E, Transmission electron microscopy images of an open-ended TNT linking two M1B26 cells,
583 with mitochondria (red asterisks). Scale bars, 5 µm (low mag), 500 nm (high mag). F,
584 Immunofluorescence images of mitochondria (green) in MCF10A-CT and M1B26 cells. Actin,
585 red; nuclei, blue. Scale bars, 20 µm. G, Immunofluorescence images of actin (red) in mammary
586 acini grown from MC26 and M1B26 cells. Scale bars, 5 µm. Right, 3D-projection of a TNT
587 linking two M1B26 cells, obtained with Zeiss ZENlite3.6 software. Actin, red; nuclei, blue. H,
588 Images of TNTs linking M1B26 (GFP, green) to normal human primary mammary cells. Actin,
589 red; nuclei, blue. Asterisks: emerging from M1B26 (green); between both cell types (red). Scale
590 bars: left, 20 µm; right, 10 µm.

591

592 **Figure 2** | TNTs link transformed and non-transformed mammary cells, favoring a directional
593 transfer of information. A, Fluorescence images of GFP-labeled-M1B26 (transformed - Tf;
594 green) and mCherry-labeled MCF10A (non-transformed - NoTf; red) cells, after 48 h in
595 coculture. Scale bars, 5 µm. B,C, Relative number of TNTs linking NoTf to Tf, or Tf to NoTf
596 cells (B) and TNT ratio defined as $\frac{NoTf>Tf}{NoTf-NoTf}$ (black arrows *vs* red lines) or $\frac{Tf>NoTf}{Tf-Tf}$ (black
597 arrows *vs* green lines) after 48h in coculture (C). Z stacks of 10 sections each were taken *per*
598 condition and 100 cells minimum were counted. TNTs were counted and measured in each Z-
599 stack. Error bars depict SD. Statistical significance was calculated using an unpaired Student's
600 two-sided t test with Welch's correction (n = 5 biological replicates; *** $p < 0.001$). D,
601 Fluorescence images of material transfer (green dots) from Tf (green) to NoTf cells.

602 Membranes, red; nuclei, blue. Scale bars: 100 µm, in zoom 20 µm. E, Time-lapse snapshots of
603 green material trafficking within a TNT bulge (*), from a (green) Tf to NoTf cells after 48 h in
604 coculture. Membranes, red; nuclei, blue. Scale bar, 100 µm; images recorded for 75 min, with
605 one image every 18 min (see Supplementary Movie 1). F, Flow cytometry analysis of an 8-day
606 coculture of green Tf and red NoTf cells, with a schematic of NoTf accepting material from Tf
607 cells (top: NoTf accept green, red cell with green dots), and Tf cells accepting material from
608 NoTf cells (bottom: Tf accept red, green cell with red dots). G,H, Quantification of the
609 percentage of exchange (G; n = 8 biological replicates) and fluorescence intensity (H; n = 7
610 biological replicates), for indicated transfer. Error bars depict SD. Statistical significance was
611 calculated using an unpaired Student's two-sided t test with Welch's correction (*** $p < 0.001$).
612 I, Schematic of the experimental design of coculture experiments. J,K, Quantification of the
613 number of acceptor cells *per* 10,000 cells (J), and fluorescence intensity (K), in standard or
614 Transwell™ cocultures, for indicated transfer involving normal human primary mammary
615 (normal) and M1B26 cells (Tf). Error bars depict SD. Statistical significance was calculated
616 using an unpaired Student's two-sided t test with Welch's correction (n = 3 biological replicates;
617 ns, not significant; * $p < 0.05$; ** $p < 0.01$).

618

619 **Figure 3** | TNT-dependent phenotypic changes of non-transformed cells acceptor of material
620 from transformed cells. A, Schematic of the experimental design: 4 cell populations, sorted by
621 flow cytometry (NoTf, Tf, NoTf in coculture without fluorescent transfer [non-transformed
622 non-acceptor cells - NoTf no accept], NoTf in coculture with fluorescent transfer [non-
623 transformed acceptor cells - NoTf accept]), underwent proteomic analyses and RT-qPCR. B,C,
624 Volcano plot (B) showing Log_2 enrichment of individual proteins in NoTf accept compared to
625 NoTf no accept cells from the same coculture (see schematic). P-value threshold was set at 0.05
626 and 0.8 for Log_2 fold change. C, To obtain a larger pool of hits, it was lowered to 0.5, generating
627 a list of 193 proteins upregulated in NoTf accept cells, used to generate the GOBP subset with
628 STRING (https://string-db.org). D,E, Box and whiskers plots of Log_2LFQ values (Protein
629 Levels) of EST1 (*CES1*), Plastin-2 (*LCP1*), Rab-6B (*RAB6B*), TRIQK (*TRIQK*) (D), and H-
630 Ras and K-Ras (E), for indicated sorted cell populations. Statistical significance was calculated
631 using one-way ANOVA with Dunnett's multiple comparison test (n = 5 biological replicates; *
632 $p < 0.05$; ** $p < 0.01$; *** $p < 0.001$; **** $p < 0.0001$). For clarity, comparisons with Tf cells
633 were omitted, and in (E), only significant comparison are shown. F,G, Immunofluorescence
634 images of actin (red) and tubulin (green) in (F) HMLE and HMLER cells, and (G) MCF10A,

635 MCF10.AT1 and MCF10.DCIS cells. Nuclei, blue. Scale bars = 20 μm. H,I, From left to right:
636 quantification of TNT number *per* cell, average length, and percentage of long TNTs in
637 indicated cell lines. Ten Z-stacks of 10 sections each were taken *per* condition and 100 cells
638 minimum *per* experiment were counted. TNTs were counted and measured in each Z-stack.
639 Statistical significance was calculated using an unpaired Student's two-sided t test with Welch's
640 correction (n = 8 and n = 5 biological replicates for HMEC-derived and MCF10A-derived cell
641 lines, respectively; ns, not significant; ** $p < 0.01$).

642

643 **Figure 4** | Expression of actors of the BMP signaling pathway is enhanced in acceptor cells
644 after TNT transfer. A, Box and whiskers plots of Log_2LFQ values (Protein Levels) of ID1,
645 Nup214, Spartin, USP15, ATF2, MAPKAPK2 and Rac1, for indicated sorted cell populations.
646 Statistical significance was calculated using one-way ANOVA with Dunnett's multiple
647 comparison test (n = 5 biological replicates; * $p < 0.05$; ** $p < 0.01$; *** $p < 0.001$; **** $p <$
648 0.0001). For clarity, only comparison between NoTf and NoTf accept cells is shown. B,
649 Immunofluorescence images of actin (red) and BMPR1b (green) in indicated cells. Nuclei
650 (blue). Scale bars, 20 μm. C, Correlative light scanning electron microscopy (SEM) of
651 BMPR1b, immunostained with Alexa Fluor®488-Fluoronanogold™ (green) in M1B26 cells.
652 From left to right: Airyscan confocal, scanning electron microscopy, zooms, correlative
653 (overlay). Scale bars, 10 μm, unless otherwise indicated. D, Immunofluorescence of actin
654 (green), after transfection with siRNA pools targeting *BMPR1b* (siBMPR1b) or *GPER*
655 (siGPER). Non-targeting siRNA: siCTRL. E, *BMPR1B* and *GPER* transcript and protein
656 expression upon their silencing (top),with siCTRL set at 1 (n = 4), and (bottom) TNT number
657 (> 8 μm) *per* cell and % of long TNTs (> 50 μm) upon indicated silencing, normalized against
658 siCTRL. Error bars depict SD. Statistical significance was calculated using an unpaired
659 Student's two-sided t test with Welch's correction (n = 4 biological replicates, *** $p < 0.001$).
660 F, Schematic of experimental design: after sorting, cell populations were either lysed at day 8,
661 and subjected to RT-qPCR for selected transcript analyses, or grown for several weeks with or
662 without BMP2/IL6, and immunoblot analyses performed at end points. G, RT-qPCR
663 measurement of BMPR1b mRNA in indicated cell populations at day 8, the expression in NoTf
664 cells (monocultures) set at 1. Statistical significance was calculated using one-way ANOVA
665 with post-hoc Tukey test (n = 5 biological replicates). For clarity, only comparison between
666 NoTf accept and NoTf cells is shown (**** $p < 0.0001$).

667

Figure 5 | Non-transformed cells acceptor of information from transformed cells *via* TNTs display preneoplastic features. A, Left, quantification of BMPR1b immunoblots performed on NoTf accept cells grown in the presence of BMP2/IL6, for indicated weeks post sorting. Box and whiskers plot of 6 biological replicates. Statistical significance was calculated using a one-way ANOVA with non-parametric Kruskal-Wallis test, and for clarity, only p-values ≤ 0.05 are indicated. Right, quantification of BMPR1b immunoblots performed on indicated cells, 14 weeks post sorting, with NoTf conditions set at 1 (n = 6 biological replicates). Statistical significance was calculated using a one-way ANOVA with post-hoc Tukey test (*** $p < 0.001$). B,C, Quantification of p-SMAD1/5/8 / SMAD1/5/8 (B) and p-p38/p38 (C) immunoblots performed on NoTf accept cells grown in the presence of BMP2/IL6, for indicated weeks post sorting. Box and whiskers plot of 6 biological replicates. Statistical significance was calculated using a one-way ANOVA with non-parametric Kruskal-Wallis test, and for clarity, only p-values ≤ 0.05 are indicated. D, RNA-sequencing results of transcriptomic expression levels of *HOXB6, CCND2, EREG* and *HRAS* in indicated cell lines (n = 3 biological replicates). Data deposited on the Gene Expression Omnibus repository, GSE186734 [5]. Error bars depict SD. Statistical significance was calculated using a one-way ANOVA with post-hoc Tukey test (* $p < 0.05$; ** $p < 0.01$; *** $p < 0.001$; **** $p < 0.0001$). E, RT-qPCR measurements of HOXB6, CCND2, EREG and HRAS mRNA in indicated cell populations, with the expression in NoTf cells set at to 1. Error bars depict SD. Statistical significance was calculated using a one-way ANOVA with post-hoc Tukey test (biological replicates: n = 8 for *HOXB6*, n = 5 for *CCND2*, n = 7 for *EREG*, n = 8 for *HRAS*). For clarity, only comparisons between NoTf, NoTf Transwell and NoTf accept cells are shown (* $p < 0.05$; ** $p < 0.01$; *** $p < 0.001$; **** $p < 0.0001$). F, Quantification of soft agar clones of indicated sorted cells, after 8, 10, 14 and 16 weeks in culture with or without BMP2/IL6 (n = 3 biological replicates). Error bars represent SD. Statistical significance was calculated using a one-way Welch and Brown-Forsythe ANOVA test (* $p < 0.05$; ** $p < 0.01$; *** $p < 0.001$; **** $p < 0.0001$). For clarity, only p-values ≤ 0.05 are indicated, and comparisons with Tf cells are omitted. G, Model depicting how TNTs might be involved in the propagation of a BMP-dependent preneoplastic state. Fibrils and fibers illustrate extracellular matrix components.

Cuella Martin *et al* Figure 1

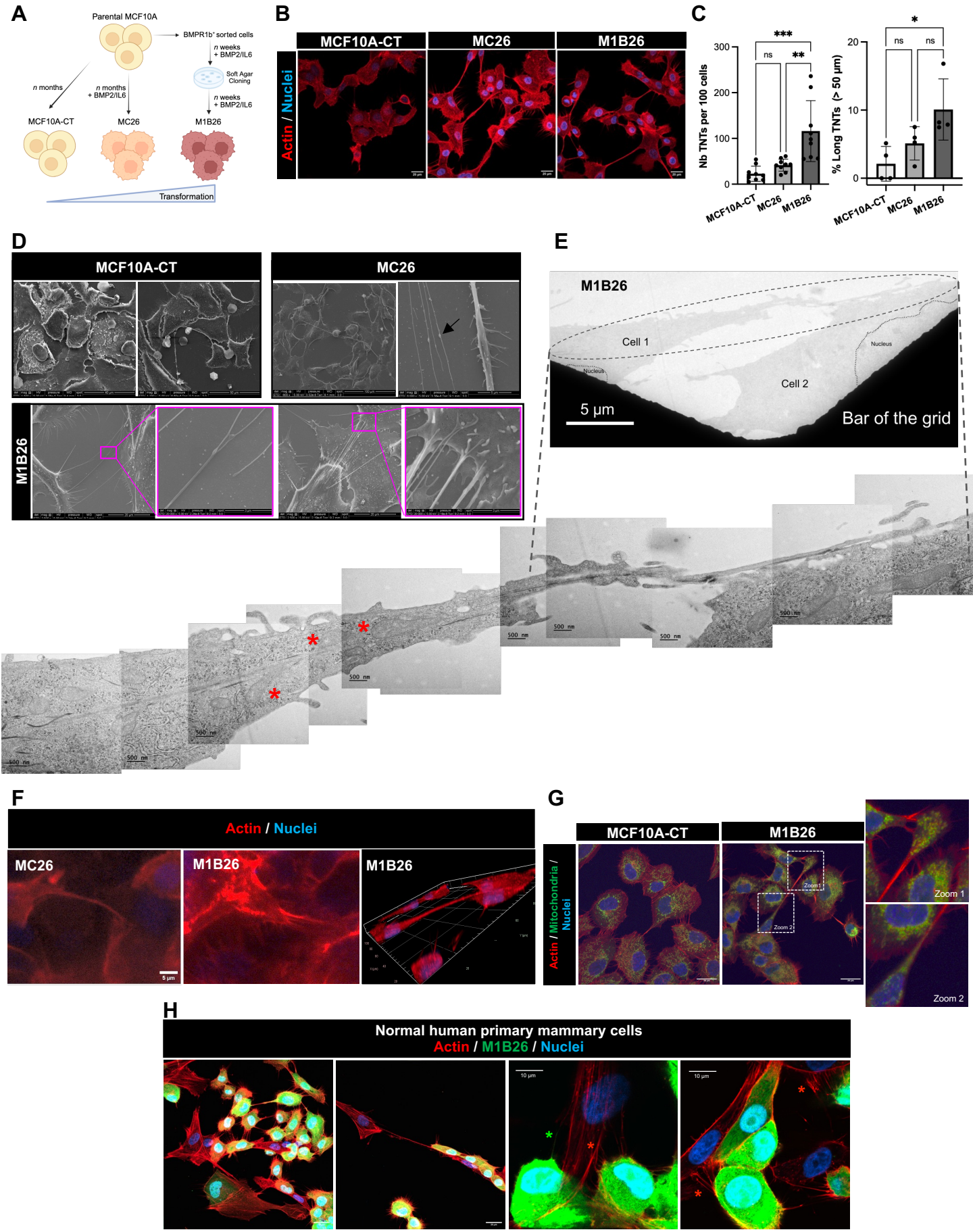

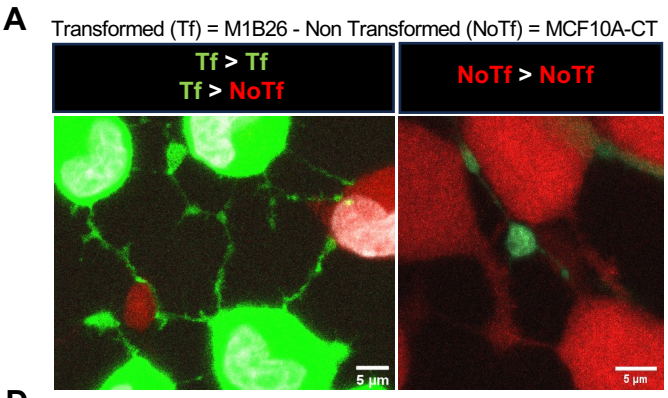

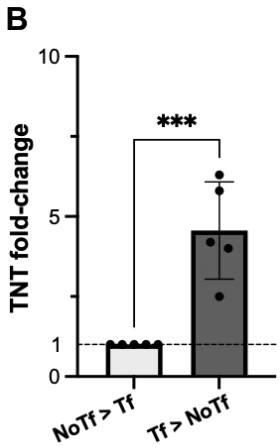

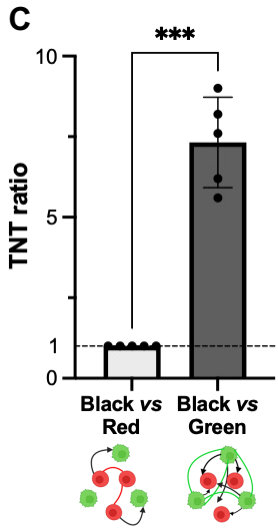

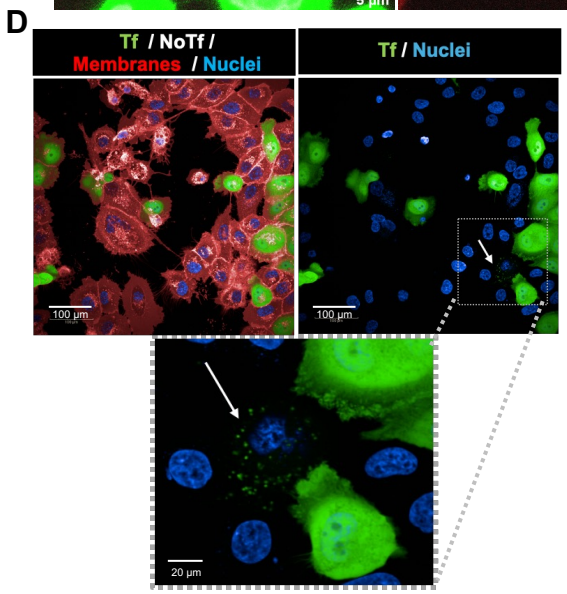

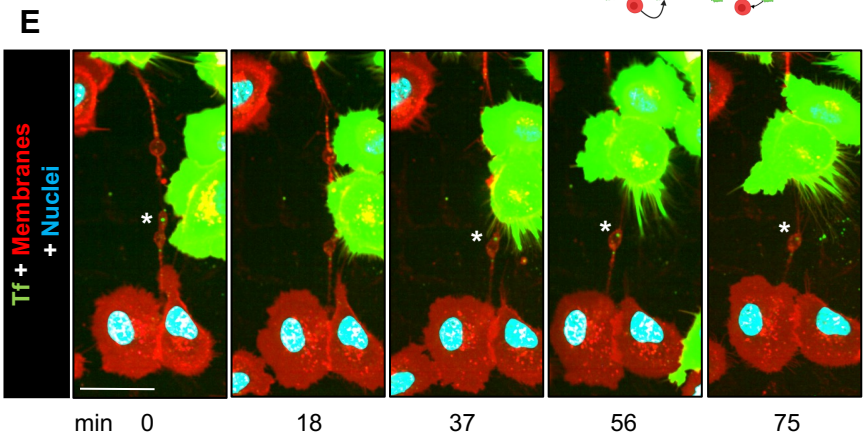

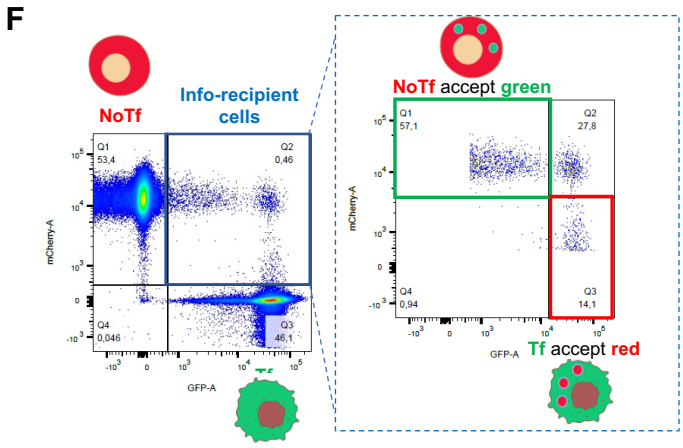

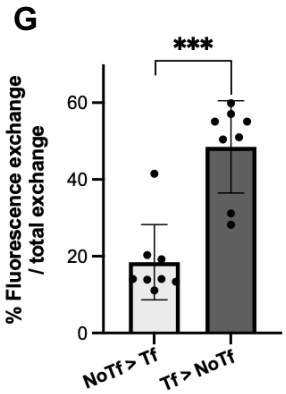

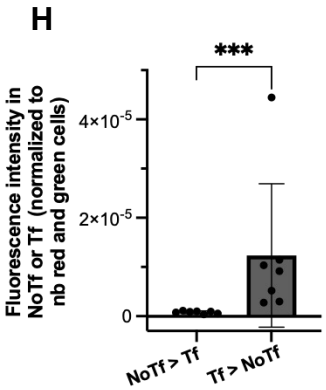

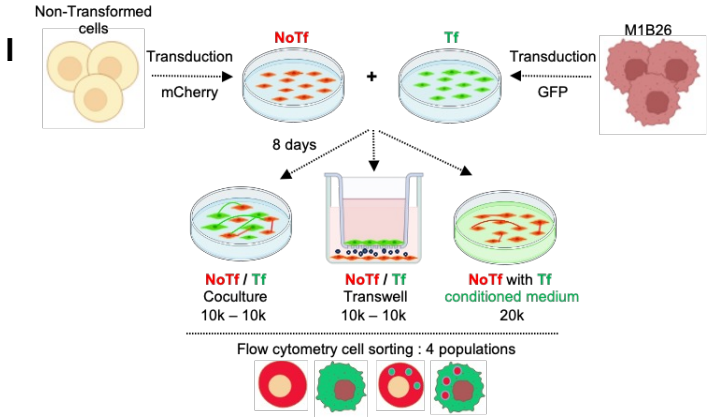

NoTf = Normal human primary mammary cells

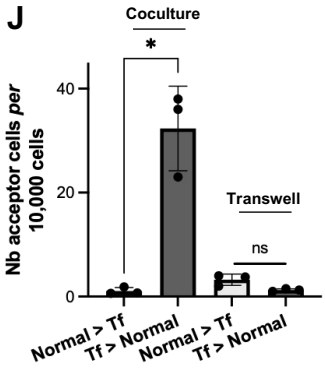

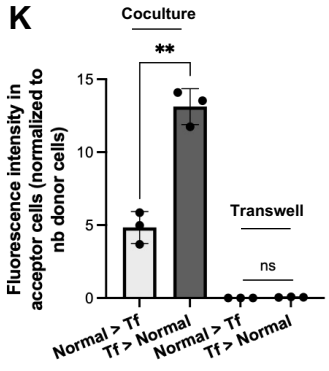

Cuella Martin *et al* Figure 3

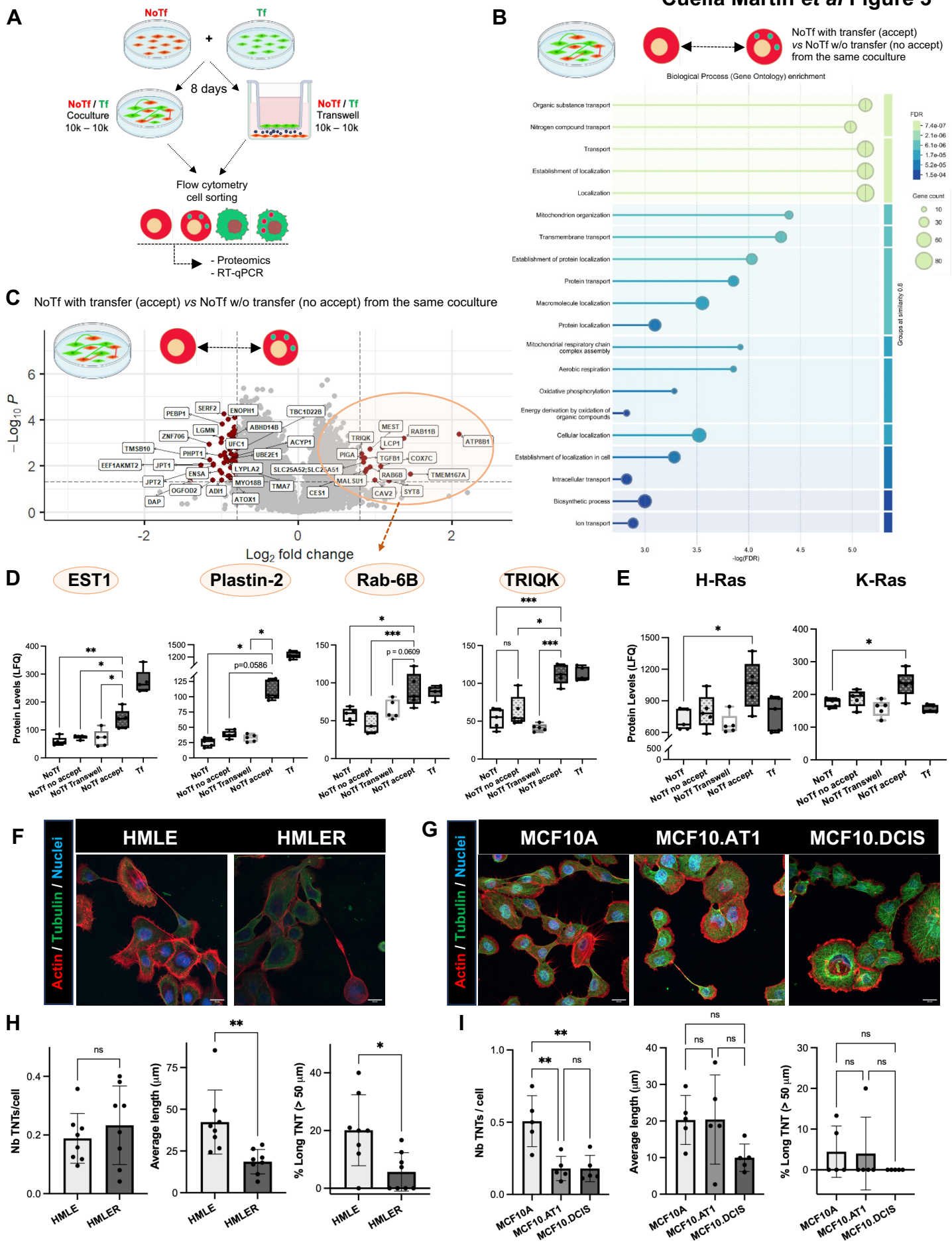

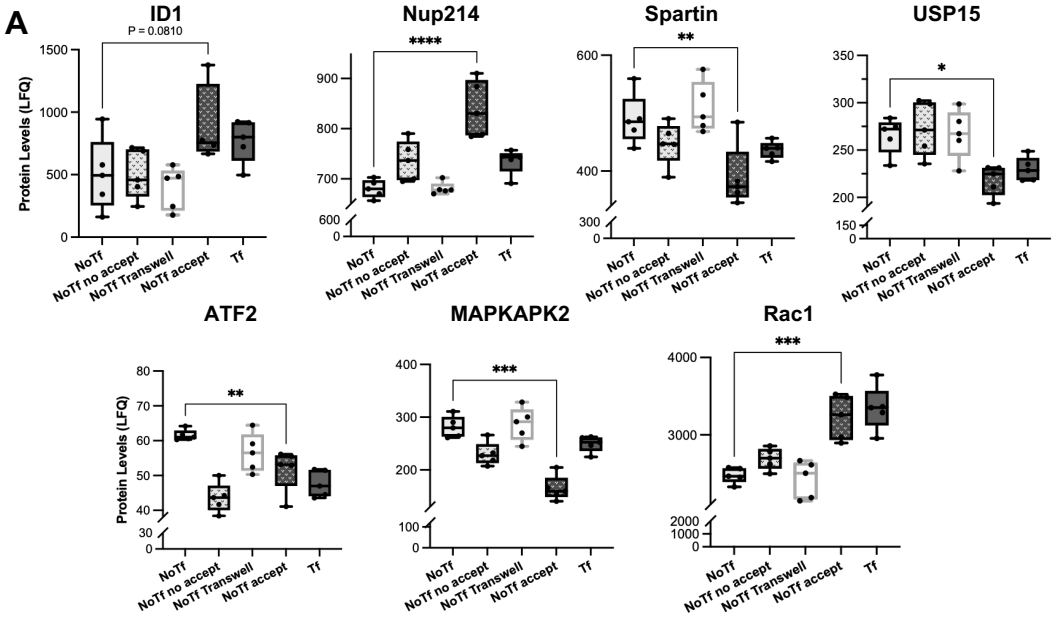
A
ID1
P = 0.0810
Nup214
****
Spartin
**
USP15
*
ATF2
**
MAPKAPK2
***
Rac1
***
Protein Levels (LFQ)
NoTf
NoTf no accept
NoTf Transwell
NoTf accept
Tf

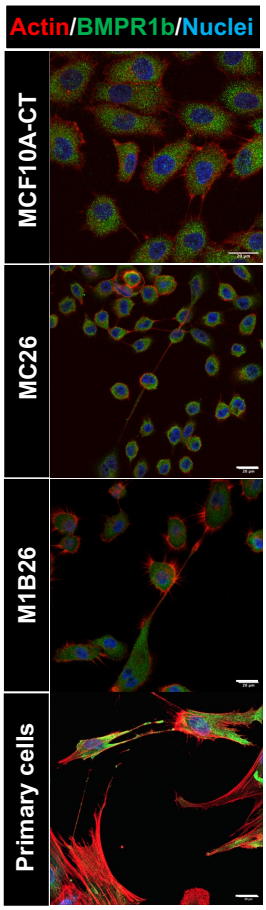
B
Actin/BMPR1b/Nuclei
MCF10A-CT
MC26
M1B26
Primary cells

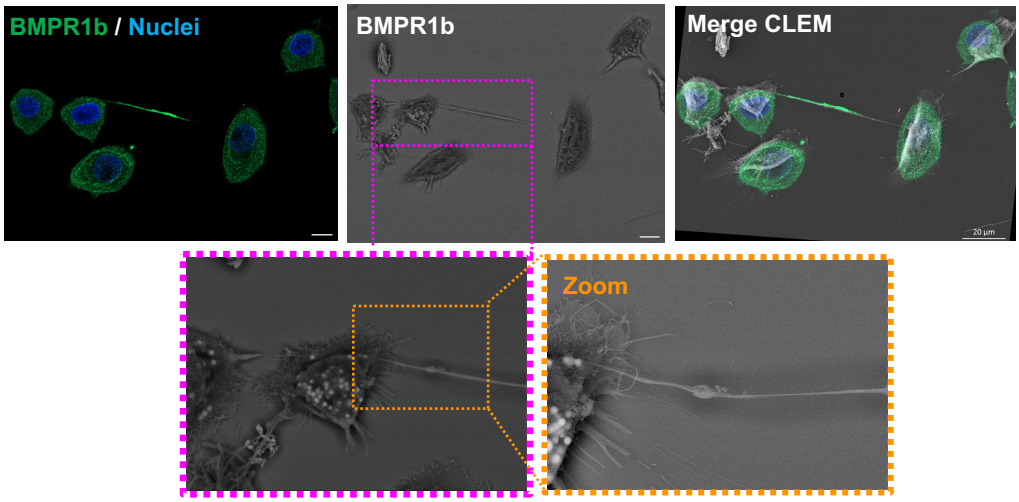
C
BMPR1b / Nuclei
BMPR1b
Merge CLEM
Zoom

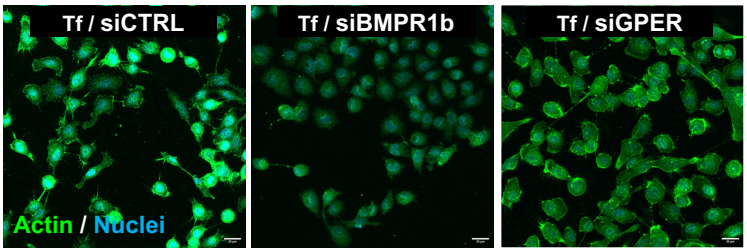
D
Tf / siCTRL
Tf / siBMPR1b
Tf / siGPER
Actin / Nuclei

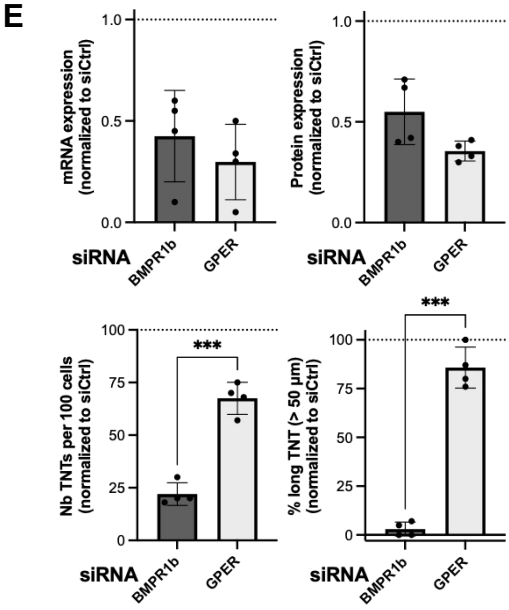
E
mRNA expression (normalized to siCtrl)
Protein expression (normalized to siCtrl)
Nb TNTs per 100 cells (normalized to siCtrl)
% long TNT (> 50 µm) (normalized to siCtrl)
siRNA
BMPR1b
GPER
***

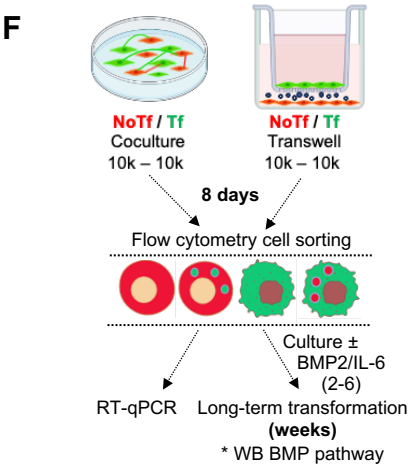
F
NoTf / Tf
Coculture
10k – 10k
NoTf / Tf
Transwell
10k – 10k
8 days
Flow cytometry cell sorting
Culture ±
BMP2/IL-6
(2-6)
RT-qPCR
Long-term transformation
(weeks)
* WB BMP pathway

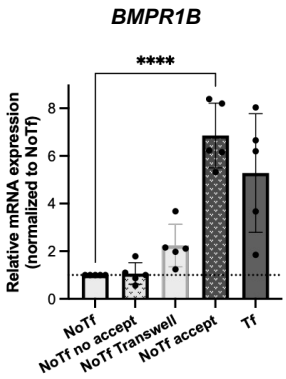
G
BMPR1B
****
Relative mRNA expression (normalized to NoTf)
NoTf
NoTf no accept
NoTf Transwell
NoTf accept
Tf

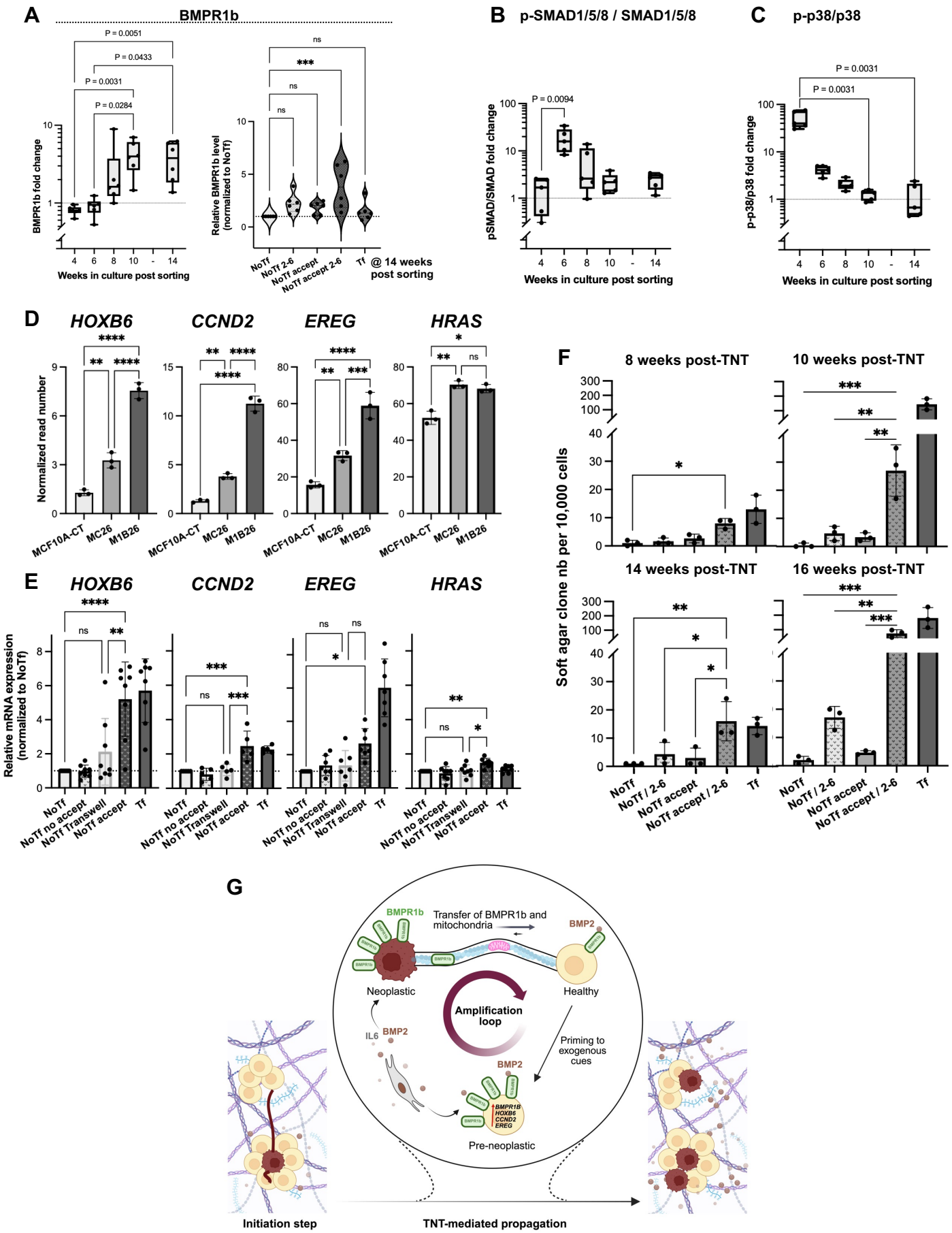
A
BMPR1b
P = 0.0051
P = 0.0433
P = 0.0031
P = 0.0284
BMPR1b fold change
Weeks in culture post sorting
ns
***
ns
ns
Relative BMPR1b level (normalized to NoTf)
NoTf
NoTf 2-6
NoTf accept
NoTf accept 2-6
Tf
@ 14 weeks post sorting
B
p-SMAD1/5/8 / SMAD1/5/8
P = 0.0094
pSMAD/SMAD fold change
Weeks in culture post sorting
C
p-p38/p38
P = 0.0031
P = 0.0031
p-p38/p38 fold change
Weeks in culture post sorting
D
HOXB6
CCND2
EREG
HRAS
Normalized read number
MCF10A-CT
MC26
M1B26
E
HOXB6
CCND2
EREG
HRAS
Relative mRNA expression (normalized to NoTf)
NoTf
NoTf no accept
NoTf Transwell
NoTf accept
Tf
F
8 weeks post-TNT
10 weeks post-TNT
14 weeks post-TNT
16 weeks post-TNT
Soft agar clone nb per 10,000 cells
NoTf
NoTf / 2-6
NoTf accept
NoTf accept / 2-6
Tf
G
BMPR1b
Transfer of BMPR1b and mitochondria
BMP2
Neoplastic
Healthy
Amplification loop
IL6
BMP2
Priming to exogenous cues
BMP2
BMPR1B
HOXB6
CCND2
EREG
Pre-neoplastic
Initiation step
TNT-mediated propagation